International Journal of Applied Earth Observations and Geoinformation 114 (2022) 103031

Contents lists available at ScienceDirect

International Journal of Applied Earth Observations and Geoinformation

journal homepage: www.elsevier.com/locate/jag

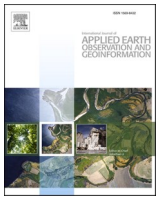

Quantifying mangrove canopy regrowth and recovery after Hurricane Irma with large-scale repeat airborne lidar in the Florida Everglades

Lin Xiong [a,*], David Lagomasino [a], Sean P. Charles [a], Edward Castañeda-Moya [b], Bruce D. Cook [c], Jed Redwine [d], Lola Fatoyinbo [c]

[a] Integrated Coastal Programs, East Carolina University, Wanchese, NC 27981, USA
[b] Institute of Environment, Florida International University, Miami, FL 33199, USA
[c] Biospheric Sciences Laboratory, NASA Goddard Space Flight Center, Greenbelt, MD 20771, USA
[d] Everglades National Park, Homestead, FL 33034, USA

ARTICLE INFO

Keywords:
Lidar
Mangrove forests
Hurricanes
Canopy height model
Recovery
South Florida
Everglades

ABSTRACT

Hurricane Irma caused significant damages to mangrove forested wetlands in south Florida, including defoliation, tree snapping, and uprooting. Previous studies have used optical satellite imagery to estimate large-scale forest disturbance and resilience patterns. However, satellite images alone cannot provide measurements of vertical mangrove structure. In this study, we used dense point cloud data collected by NASA Goddard's LiDAR, Hyperspectral, and Thermal (G-LiHT) airborne imager before (March 2017) and after (December 2017 and March 2020) Hurricane Irma to quantify the recovery, or lack thereof, of the three-dimensional (3D) mangrove forest structure. Recent resilience and vulnerability models developed from Landsat time series following the storm were used to group the lidar data into distinct disturbance-recovery classes. We then analyzed lidar-based forest canopy within each of the recovery classes to test a suite of forest structural characteristics. Our results indicate that 77.0 % of the survey area experienced canopy height loss three months after Hurricane Irma, whereby the majority of canopy height loss occurred in areas with the tallest mangrove forests (i.e., 15–25 m tall). Our analysis shows that the mangrove canopy height in South Florida increased by an average 0.26 m from December 2017 to March 2020, with most of the forest (84.7 % of the survey area) experiencing canopy height regrowth. However, only 38.1 % of the survey area has recovered to pre-storm canopy height. The distribution of canopy height was significantly altered by Hurricane Irma in the low and intermediate resilience classes, but were not significantly different 2.5 years later. Indeed, in areas of low resilience, little to no vertical change has occurred suggesting the absence of canopy regrowth and natural regeneration. Conversely, mangroves in high resilience class, which are dominated by shorter canopies (<5 m), were not heavily damaged by the storm and have maintained the same structural attributes as those before Hurricane Irma. Our findings highlight that hurricane disturbances significantly alter mangrove forest canopy structure, but recovery of vertical structure varies by resilience classes, species composition, and canopy height.

1. Introduction

Mangroves are forested wetlands comprised of trees and shrubs that grow along low-lying coastlines in tropical and subtropical latitudes, and support the natural environment and human communities through a wealth of ecosystem services including carbon storage, sequestration, habitat, water quality, and coastal protection (Walters et al., 2008; Polidoro et al., 2010; Donato et al., 2011; Lee et al., 2014; Friess et al., 2019; Menéndez et al., 2020). Globally, mangrove forests account for 11 % of the terrestrial carbon that is transferred to the ocean although they only comprise 0.1 % of the continental surface, indicating their significant contribution to carbon biogeochemistry in the coastal zone (Twilley et al., 1992; Jennerjahn and Ittekkot, 2002; Bouillon et al., 2008; Alongi, 2020). For decades, mangroves around the world have experienced rapid declines as a result of human activities, climate change, and sea level rise (Polidoro et al., 2010; Thomas et al., 2017; Goldberg et al., 2020). Although human impacts account for the majority of global mangrove losses, climatic factors (e.g., shoreline erosion, hurricanes,

* Corresponding author.
E-mail address: xiongl21@ecu.edu (L. Xiong).

https://doi.org/10.1016/j.jag.2022.103031
Received 31 May 2022; Received in revised form 17 September 2022; Accepted 19 September 2022
Available online 25 September 2022

droughts) account for ~ 11 % of global mangrove losses (Goldberg et al., 2020), with extreme weather events (e.g., hurricanes) causing widespread, but localized dieoffs (Abhik et al., 2021; Lagomasino et al., 2021). During tropical cyclones, mangroves can also help to stabilize the shoreline and protect coastal areas from powerful winds and storm surges by reducing the effects of flooding and economic damages to inland infrastructure in coastal areas (Gedan et al., 2011; Del Valle et al., 2020; Menéndez et al., 2020).

One of the top natural disturbances on mangroves are tropical cyclones, which have caused the highest instances of reported mangrove mortality area around the world since the 1960s (Sippo et al., 2018). The direct and indirect impacts of tropical cyclones can change forest structure (Rivera-Monroy et al., 2019), alter soil and hydrologic conditions (Castañeda-Moya et al., 2010, 2020; Krauss and Osland, 2020), as well as forest productivity and carbon storage (Danielson et al., 2017; Rasquinha and Mishra, 2021; Zhao et al., 2021). These alterations to the ecosystem from cyclones can have both negative and positive consequences. In extreme cases where strong cyclones make landfall, mangroves can rapidly transition from forest to mudflat as a result of mass tree mortality. The initial tree mortality can range from 0 to 100 % right after the storm and vary among different mangrove tree species, height classes, and ecotypes (Smith et al., 1994; Cahoon et al., 2003; Ross et al., 2006; Imbert, 2018). In addition, continued mortality can occur for months after the cyclone (Cahoon et al., 2003; Radabaugh et al., 2018; Rivera-Monroy et al., 2019). This delayed mortality, which is linked with thick hurricane-induced sediment deposition, can increase mortality by 9 %–17 % in the 3 to 9 months following the disturbance (Radabaugh et al., 2020). The loss of the vegetation and the increased instability of the soils can lead to rapid rates (~11 mm yr^{-1}) of shallow subsidence in basin mangrove forests (Cahoon et al., 2003) and eventually transition into mudflats (Smith et al., 2009; Osland et al., 2020). However, in most cases mangroves generally recover within a few years following cyclone disturbances (Danielson et al., 2017; Imbert, 2018; Rivera-Monroy et al., 2019). Indeed, recovery of the forest can be facilitated by an increase in phosphorus (P)-rich mineral sediments deposited by hurricanes into mangrove soils, which enhance plant P uptake and productivity following disturbance (Castañeda-Moya et al., 2010, 2020).

Numerous studies have been conducted to measure the impact and recovery of mangrove forests following major hurricanes with remote sensing methods (e.g. Heumann, 2011; Kuenzer et al., 2011; Pham et al., 2019; Wang et al., 2019; Maurya et al., 2021). Satellite remote sensing can directly measure evapotranspiration (ET), radiation, and other energy balance parameters and investigate how they respond to cyclones (Ceron et al., 2015; Lagomasino et al., 2015; Yagci et al., 2017). Daily MODIS (Moderate Resolution Imaging Spectro-radiometer) imagery has been used to measure changes in the Enhanced Vegetation Index (EVI) and studies have found that active leaf area began to recover 1 year after Hurricane Wilma in 2005 but overall carbon uptake and canopy greening was still below pre-storm conditions 5 years post-disturbance (Barr et al. 2012). Similarly, Landsat observations have been critical for mapping the distribution and change of mangrove forests in Everglades National Park (ENP) over time. For instance, from 1985 to 2017, mangrove coverage has increased by 10.2 %, although significant decreases do occur during hurricane years (Han et al., 2018; Charles et al., 2021). Landsat imagery can also be used to quantify the mangrove forest damage following cyclones (Kovacs et al., 2001; Svejkovsky et al., 2020; Taillie et al., 2020; Lee et al., 2021) and to develop risk models to hurricane impacts (C. Zhang et al., 2019). Most of these studies have focused on the landscape-scale variability and have provided important information on the environmental conditions that influence damage and recovery patterns. However, a critical missing piece, particularly in response to catastrophic events, has been capturing the vertical changes of the forest that provides information on how the canopy restructures itself after a disturbance, that are not readily captured by satellite observations.

Lidar (light detection and ranging) is an active remote sensing technique that has been widely used to measure three-dimensional (3D) forest structure such as canopy height, canopy cover, Leaf area index (LAI), basal area, and crown diameter (Dubayah and Drake, 2000; Lim et al., 2003; Zimble et al., 2003). Spaceborne lidar (e.g., GLAS, GEDI, ICESat-2, etc.), airborne laser scanning (ALS), ground-based lidar or Terrestrial laser scanning (TLS) can measure and monitor forest structure at different spatial and temporal resolutions (Lefsky et al., 2002; Zhang et al., 2008; E. Feliciano, 2015; Fatoyinbo et al., 2018; Stovall et al., 2021). One of the biggest advantages of lidar is that it can detect multiple pulse returns from the canopy top, sub-canopy, and ground surface over a relatively small footprint. Digital Surface Models (DSMs) and Digital Terrain Models (DTMs) can then be generated from the lidar point clouds. Canopy height models (CHMs), which are common and basic products for a variety of forestry applications, are calculated by subtracting DSMs from the DTMs. The majority of studies have focused on a single time period of lidar data to estimate canopy height or forest biomass (e.g. Drake et al., 2002; Lefsky et al., 2005; Kronseder et al., 2012; Lu et al., 2020), but relatively few studies have analyzed multiple lidar time series focused directly on hurricane disturbances (Zhang et al., 2008; Lagomasino et al., 2021; Leitold et al., 2021). Most lidar surveys have only been repeated once and generally focus on forest dynamics over relatively small areas 400 ha to 20,000 ha (Vepakomma et al., 2008; Hudak et al., 2012; Andersen et al., 2014; Dalponte et al., 2019). Even fewer studies have analyzed data from lidar surveys more than three times which have focused specifically on upland forests (Zhao et al., 2018; Leitold et al., 2018, 2021).

Airborne lidar surveys can cover large areas in size ranging in the thousands of square kilometers, augmenting *in-situ* observations that are limited by accessibility of field sites, cost, and labor. For example, lidar data was used to quantify the increase in canopy gaps from 1 to 2 % formed by lightning strikes to 12 % that were formed by Hurricane Wilma in ENP (Zhang, 2008, Zhang et al., 2008). Repeat lidar surveys can also map fine-scale forest dynamics such as above ground biomass changes through time over large spatial scales (Hudak et al., 2012; Meyer et al., 2013; Réjou-Méchain et al., 2015; Wedeux et al., 2020; Leitold et al., 2021). Canopy height changes, gap dynamics, tree growth, and mortality can be resolved with very high-resolution point cloud. Comparing and combining airborne lidar and satellite-based remote sensing data can provide more accurate and robust methods to assess disturbances in mangrove forests (Zhang et al., 2019b; Taillie et al., 2020; Lagomasino et al., 2021). But there are few continuous and large-scale repeat lidar datasets to study these responses in physical damage and recovery of mangrove forests after hurricanes. Therefore, several NASA projects have supported numerous recent airborne campaigns in South Florida that have resulted in the largest collections of lidar data over mangrove forests that coincide before and after a major hurricane.

The objective of this study is to quantify the long-term structural changes in mangrove forests of South Florida caused by Hurricane Irma in September 2017. The specific questions that we address are: (1) how long does it take for canopy height to recover after a catastrophic cyclone? (2) are recovery rates different between mangrove species and resilience classes following cyclone damage? We use dense point cloud data acquired from repeated surveys by NASA Goddard's LiDAR, Hyperspectral, and Thermal (G-LiHT) airborne imager (Cook et al., 2013) in March 2017 (6 months before Hurricane Irma), December 2017 (3 months after Hurricane Irma), and March 2020 (2.5 years after Hurricane Irma). The total wetland area of each lidar survey was over 130,000 ha in South Florida and high-resolution CHMs (1 m by 1 m) were generated for 3D changes analyses, and more specifically, vertical attributes of mangrove forests to help us better understand their long-term response by considering relationships with diversity, vulnerability, and resilience to hurricane impacts at a large scale.

2. Materials and methods

2.1. Study area

The study area is located in South Florida, including Everglades National Park (ENP) and Ten Thousand Islands, which are the major coastal regions within the greater Everglades ecosystem (Fig. 1). The ENP has the largest contiguous protected mangrove forests (144, 447 ha) in the continental USA (Simard et al., 2006) but has undergone compartmentalization over 20th century and reduced water flow through the ecosystem. The Comprehensive Everglades Restoration Plan (CERP) written in 2000, set aside more than $10.5 billion to restore and preserve the Everglades ecosystem over the next thirty years (https://npshistory.com/brochures/ever/fs-cerp.pdf). Only four mangrove species are found in ENP although over seventy species exist worldwide (Duke et al., 2017): *Avicennia germinans* (black mangrove), *Laguncularia racemosa* (white mangrove), *Rhizophora mangle* (red mangrove), and the mangrove associate *Conocarpus erectus* (buttonwood). The range and distribution of mangroves species in ENP are related to soil elevation, hydrology, the magnitude and interaction of environmental gradients including resources (e.g., nutrients, light), regulators (i.e., soil salinity, sulfide), and hydroperiod (e.g., frequency, duration, and depth of water), and connectivity with saltwater and freshwater resources (Lugo and Snedaker, 1974; Chen and Twilley, 1999; Twilley and Rivera-Monroy, 2005, 2009; Castañeda-Moya et al., 2013). Rainfall varies seasonally in South Florida, whereby the majority of rain, over 60 % of the annual rainfall, occurs within the wet season from May to October compared to the dry season from November through April (Duever et al., 1994; Abtew et al., 2005; Dessu et al., 2018). The wet season rainfall can also be punctuated with tropical cyclone activity, while during the early dry season, the region experiences the winter frontal season (Duever et al., 1994).

The Atlantic basin is an active tropical cyclone zone and can generate powerful hurricanes that stochastically, but regularly impact south Florida. Hurricanes are much more frequent in Florida than in other states because they can come from the Gulf of Mexico, Caribbean Sea or the Atlantic Ocean (Malmstadt et al., 2009). Hurricanes hit Florida on average every-five years (Keim et al., 2007) with a ~ 12-year major hurricane recurrence interval (Zhang et al, 2008). On September 10, 2017, Hurricane Irma made landfall in southwest Florida as a Category 3 cyclone with maximum sustained winds of ~ 50 m/*sec* (116 mph). The strong winds pushed the maximum water level, a combination of tide and storm surge, 2–3 m above the ground along the southwest coast of Florida, in addition to heavy rainfall (25–38 cm) that caused excessive flooding (Cangialosi et al., 2018). Strong winds, storm surge, and flooding can cause extensive damage to mangroves by stripping leaves and snapping or uprooting trees. The frequency and intensity of hurricanes that hit south Florida, combined with accelerated rates of sea level rise in the region (Wdowinski et al., 2016) and rapid coastal urban expansion (Rifat and Liu, 2019) make it a unique location to study the direct and indirect impacts of storms on mangrove forest structure and function and environmental attributes.

2.2. Data collection and methods

2.2.1. G-LiHT airborne lidar data and processing

Lidar data were collected using NASA Goddard's Lidar Hyperspectral, and Thermal (G-LiHT) multi-sensor airborne imaging system, which simultaneously measures vegetation structure, foliar spectra, and surface temperatures (Cook et al., 2013). During 2017, the G-LiHT lidar

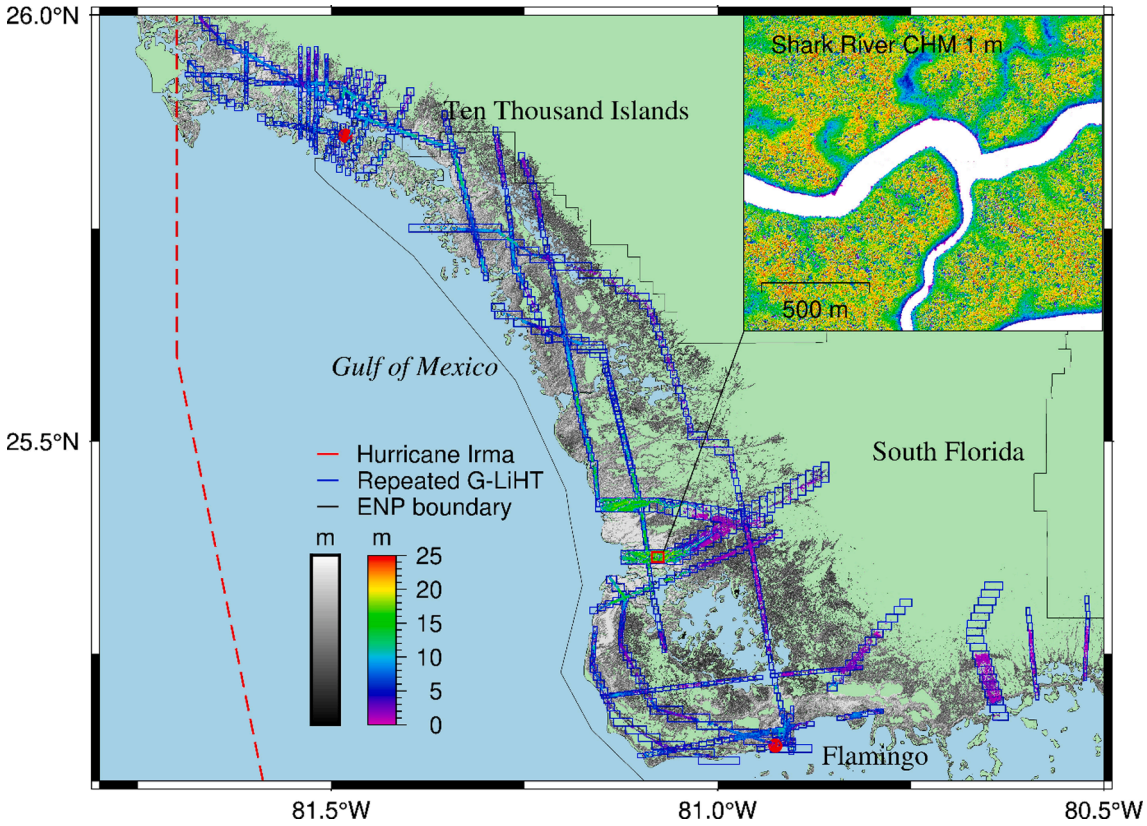

Fig. 1. Mangrove height map for South Florida. Red dashed lines show the path of Hurricane Irma in 2017. Blue polygons indicate repeat G-LiHT surveys over mangrove forests (March 2017, December 2017, and March 2020). Canopy height model (CHM) in grey color is from Simard et al. (2019) for the nominal year 2000 and CHM in rainbow color is from G-LiHT data for the year 2020. Red rectangle shows boundary of the Canopy Height Model (CHM) in the subfigure. Red dots show the locations of Ten Thousand Islands (TTI) and Flamingo, where high-resolution orthophotos were taken (Fig. 3). (For interpretation of the references to color in this figure legend, the reader is referred to the web version of this article.)

system was improved by upgrading the existing Riegl model VQ-480 lidar to a VQ-480i (Horn, Austria); adding a second VQ-480i lidar; and upgrading the GPS-INS to an Applanix POS AV V6 (Richmond Hill, Ontario, Canada). Each lidar emits a 1550 nm laser pulse with 0.3 mrad beam divergence, which produces a footprint of ~ 10 cm diameter at a nominal acquisition height of 335 m Above Ground Level (AGL). A laser pulse repetition frequency of 300 kHz and nominal air speed of 130 kts produces a lidar sampling density of ~ 12 laser pulses m^{-2}. The high density of small footprint lidar measurements provides a very detailed 3D structure of mangrove forests, which is not possible using space-based systems with greater pulse duration, larger target footprints, and sparser sampling. Laser energy at 1550 nm is strongly attenuated by water and does not penetrate open water bodies. Open water body elevations were measured by specular reflection of laser energy in the near-nadir direction and from areas where wind and turbulence created waves or ripples on the water surface.

G-LiHT GPS-INS data were post-processed with Applanix POSPac Mobile Mapping Suite 8 georeferencing software (MMS; Richmond Hill, Ontario, Canada) and Trimble Post-Processed CenterPoint RTX global GNSS correction service (PP-RTX; Sunnyvale, CA, USA), which provides cm-level positioning accuracy by utilizing a global network of tracking stations to reduce ephemeris, timing, and atmospheric uncertainties. All geographic coordinates were projected in Universal Transverse Mercator (UTM Zone 17 N for south Florida), using WGS-84 (World Geodetic System 1984) and EGM96 (Earth Gravitational Model 1996) as horizontal and vertical datum, respectively.

Riegl's RiPROCESS software was used to manage, process, analyze and visualize Level 0 data from the laser scanner and GPS-INS. Data processing involved data import and calibration; waveform analysis and correction for Multiple-Time-Around (MTA) ambiguities; georegistration of discrete returns using precision GPS-INS data; and export of point cloud data. Higher-Level G-LiHT products (e.g., aircraft trajectory in ASCII format; LAS files with AGL height and classification for each return; gridded elevation and AGL height models, apparent reflectance, plot-scale statistics, and change maps in GeoTIFF format) were produced by algorithms custom coded in IDL-ENVI (Interactive Data Language and Environment for Visualizing Images; Exelis Visual Information Solutions, Boulder, CO, USA). These workflows are described in Cook et al. (2013) and available for visualization and downloading through the G-LiHT webpage (https://gliht.gsfc.nasa.gov) and interactive data center (https://glihtdata.gsfc.nasa.gov).

Ground returns were classified using a Progressive Morphological Filter (Zhang et al., 2003), and a Triangulated Irregular Network (TIN) surface was used to interpolate the ground elevation and create a Digital Terrain Model (DTM) for each 1 m^{-2} grid cell without ground returns. A Canopy Height Model (CHM) was generated by creating a TIN from the highest non-ground returns, interpolating the elevations to grid cell centroids, and subtracting canopy elevation, or Digital Surface Model (DSM), from the DTM to compute height in units Above Ground Level (AGL). An example of post-hurricane mangrove DTM, CHM and lidar point cloud are shown in Fig. 2.

Three repeat G-LiHT airborne lidar surveys were conducted over the Florida Everglades. To reduce uncertainty between flights, we used the same G-LiHT v.2 system flying at a similar altitude (~335 m) with the exact same sensor configuration (Riegl VQ 480i) and similar swath overlap ratio (~30 %) during the three repeated surveys. Repeat acquisitions over stationary targets without trees (e.g., buildings, roadways) demonstrated a swath-to-swath repeatability of 10 cm (1σ) absolute elevation following boresight alignment, and similar differences were observed between subcanopy ground elevations computed for March 2017 and December 2020 (data not shown). The first flight occurred in March 2017, the second 3 months after Hurricane Irma in December 2017, and the third in March 2020. The surveyed area for each flight campaign covered an approximate area of over 130,000 ha across south Florida. This is one of the largest collections of airborne lidar data that has been acquired within months before and after a major hurricane, capturing the immediate impacts of the storm, as well as the long-term recovery. All CHMs are available for download through the G-LiHT webpage (https://G-LiHT.gsfc.nasa.gov) and the point cloud data are also distributed by LP DAAC (https://lpdaac.usgs.gov/). There are

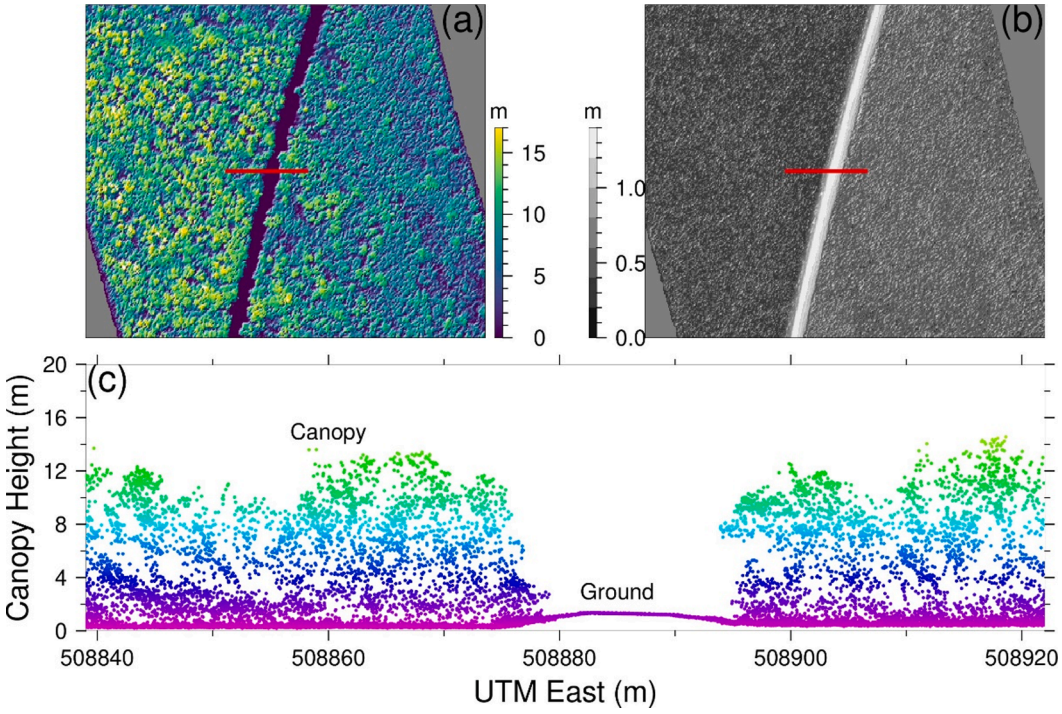

Fig. 2. Airborne lidar data was collected over South Florida three times between 2017 and 2020. An example (a) Canopy Height Model (CHM), (b) Digital Terrain Model (DTM), and (c) point cloud profile of mangrove forests across the road near Flamingo acquired on December 6, 2017. Red lines in (a) and (b) show the forest point cloud profile location in (c). (For interpretation of the references to color in this figure legend, the reader is referred to the web version of this article.)

1983, 1453, and 930 CHMs in March 2017, December 2017, and March 2020, respectively. The length of each CHM is ~ 1 km, but the width of CHM varies depending on the swath configuration during the flight.

2.2.2. Canopy structure analysis

To quantify the immediate and long-term recovery trajectories of mangrove canopy height, we calculated the difference of CHMs for post-Irma damage (March 2017 – December 2017), 2.5 years of regrowth (December 2017 – March 2020), and post-Irma recovery (March 2017 – March 2020) at 1 m resolution on mangrove forests across the Everglades. We grouped the CHMs based on the resilience and vulnerability models developed from Landsat time series following Hurricane Irma (Lagomasino et al., 2021). The mangrove forest resilience classes are separated into three categories: low, intermediate, and high and are based on the magnitude of forest greenness loss and the slope of the Normalized Difference Vegetation Index (NDVI) following the storm (Lagomasino et al., 2021). For example, in low resilience regions, the recovery time is over 15 years, whereas the recovery time for high resilience class is within 5 years. We used gdalwarp in gdalUtils library of the R statistics software to transform the coordinates system of the resilience map from WGS84 to UTM zone 17 N. Resolution of the resilience map is upsampled from 30 m to 1 m using projectRaster with nearest neighbor interpolation method. Then the reprojected resilience map in UTM coordinates is used as a mask to group raster cells in CHMs into low, intermediate, and high resilience classes. Density plots of canopy height in March 2017, December 2017, and March 2020 are calculated and presented for each resilience class.

Using the CHM time series, we quantified the changes in canopy height regrowth according to height classes and species classes. The pre-storm mangrove canopy height map was subdivided into five classes (0–5 m, 5–10 m, 10–15 m, 15–20 m, and > 20 m) to compare the mangrove forest structure and quantify the damage and regrowth in each class. CHMs in March 2017 are regarded as the pre-storm canopy map and processed as masks for CHMs in December 2017 and March 2020. Statistical metrics including mean, area, and standard deviation are calculated for each class. Vegetation maps developed by the National Park Service (i.e., Region 2, 3, and 4) (Ruiz et al., 2021) were used to identify key mangrove vegetation communities. The Everglades vegetation mapping project was performed in 2021 and covered around 1.1 million acres of the whole Everglades National Park. Very high resolution (30 cm) false color aerial images are superimposed by a 50 m by 50 m grid cell. The images are displayed in 3D using stereoscopic techniques and used to identify dominant and secondary vegetation species in each cell. The vegetation map is assessed by 1,014 random ground-truth points and the classification accuracy is 89.2 %. In total the vegetation map contains 286 discreet thematic classes. The vegetation map is resampled in 30 m resolution to match the resilience map resolution. We considered five vegetation cover classes: 1) *A. germinans*, 2) *L. racemosa*, 3) *R. mangle*, 4) *C. erectus*, and 5) a single mixed species mangrove class, each of them grouped by their dominant species classification regardless of the secondary species. Each species class distribution was used as a mask to filter G-LiHT data that was observed within the respective class. Density plots and statistical analyses for those five vegetation cover classes are presented.

2.2.3. Statistical significance tests

We tested the significant differences of canopy height data among different dominant mangrove species classes using the Tukey HSD (honestly significant difference) Test in R (version 4.1.3). The Tukey HSD test can determine whether each possible pair of datasets are statistically significant or not, particularly when there are three or more groups in the datasets. The main idea of the test is to calculate absolute mean difference $|\overline{X}_1 - \overline{X}_2|$ between a pair of datasets and divide each of them by the standard error of the mean (δ) of the sum of the means (Eq. (1)). The value q from the test will compare to the values from a studentized range distribution and determine if the two means are significantly different at a confidence level of 95 %.

$$q = |\overline{X}_1 - \overline{X}_2|/\delta \quad (1)$$

In addition, we conducted a two-sided Kolmogorov-Smirnov statistics (KS) test in R (version 4.1.3) to measure the difference in the canopy height frequency distribution curves between pre-storm, post-storm, and regrowth in different resilience classes and dominant mangrove species classes. The KS test is one of most widely used methods to determine whether two sample datasets have the same probability distribution and allows for discontinuity, heterogeneity, and dependence. It can quantify the distance between empirical functions of two sample datasets. The critical value is based on a 95 % of confidence interval and size of sample datasets using the following equation:

$$KScrit = 1.36/\sqrt{n} \quad (2)$$

where KScrit is the critical value for the KS test and n is the sample size.

3. Results

3.1. Canopy structural changes by resilience classes

G-LiHT flights covered mangrove forests in Ten Thousand Islands, Shark River, Harney River, and Cape Sable/Flamingo (Fig. 1). Damage and recovery can be directly visualized though orthomosaic photos of mangrove forests close to Flamingo, collected before and after Hurricane Irma (Fig. 2a, b, and c). Hurricane Irma caused widespread damage to the forest in the form of defoliation, tree uprooting, broken branches and toppled trees. Different trajectories of mangrove forest recovery can be seen along the road in Flamingo showing areas of dieback and recovery (Fig. 3c). Spatial patterns of mangrove forest disturbance can be observed in Ten Thousand Islands where partial recovery of the mangrove green canopy occurred inland, but the shoreline boundary still showed little green canopy recovery (Fig. 3d, e, and f).

Canopy Height Models across mangrove forests in South Florida were derived from G-LiHT data pre-Irma (CHM_{Mar17}), three months post-Irma (CHM_{Dec17}), and 2.5 years post-Irma (CHM_{Mar20}). Our results show that 84.7 % of the surveyed mangrove forests experienced regrowth after Hurricane Irma. Areas that experienced regrowth occupied 85.0 % and 95.1 % of the high and intermediate resilience classes, respectively (Fig. 4). However, canopy height continued to decrease after the initial disturbance in the low resilience class (over 50 %), as clearly noted in the Ten Thousand Islands and Flamingo sites (Fig. 4).

We measured changes in canopy height of mangrove forests in South Florida from CHM_{Mar17} to CHM_{Mar20} (Fig. 5). Only 38.1 % of mangrove forests that were surveyed by G-LiHT have recovered to pre-storm canopy height and nearly all mangroves within high resilience class showed either no damage or recovery back to pre-storm conditions. Indeed, only 9.6 % of mangroves within the low resilience class have recovered by March 2020 (Table 1). In the low resilience class around Ten Thousand Islands and Flamingo (Fig. 5), canopy height was still on average 5.69 to 5.87 m shorter than before Hurricane Irma. The intermediate resilience class around Harney River and Shark River, showed partial recovery of 27.5 % and 11.7 %, respectively. Interestingly, rapid vertical growth of ~ 1 m per year was noted in interior mangrove areas along Harney River, approximately 1.5 km south of WSC-9 site, which experienced little or no damage in canopy height after the hurricane (Fig. 5).

Density plots of canopy height vary across the three resilience categories and presented different change trajectories in response to Hurricane Irma (Fig. 6). In low resilience classes, the density, or occurrence of mangroves between 10 and 25 m tall decreased substantially (23.0 % to 14.7 %) while the density of mangroves below 5 m increased from 23.1 % to 40.3 % (Fig. 6a). In the intermediate resilience classes, the density of mangroves between 10 and 25 m tall decreased substantially (40.1 %

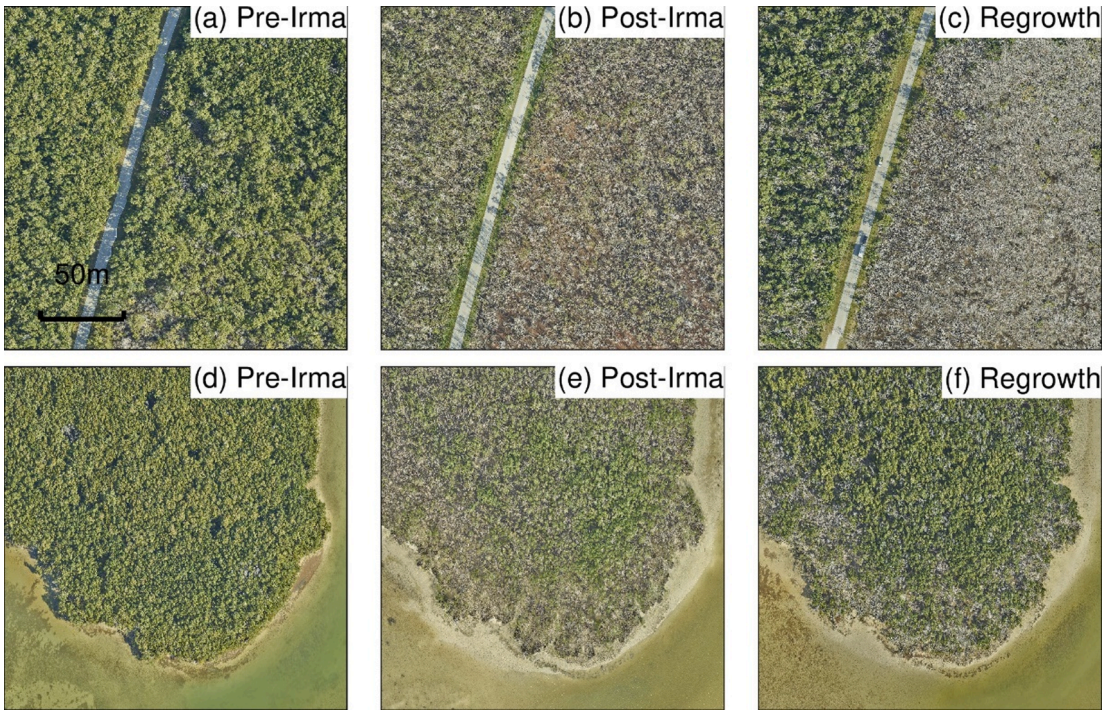

Fig. 3. High-resolution orthophotos of Flamingo (a, b, c) and Ten Thousand Islands (TTI; d, e, f) pre-Irma (March 2017), post-Irma (Dec 2017), and regrowth (March 2020) periods.

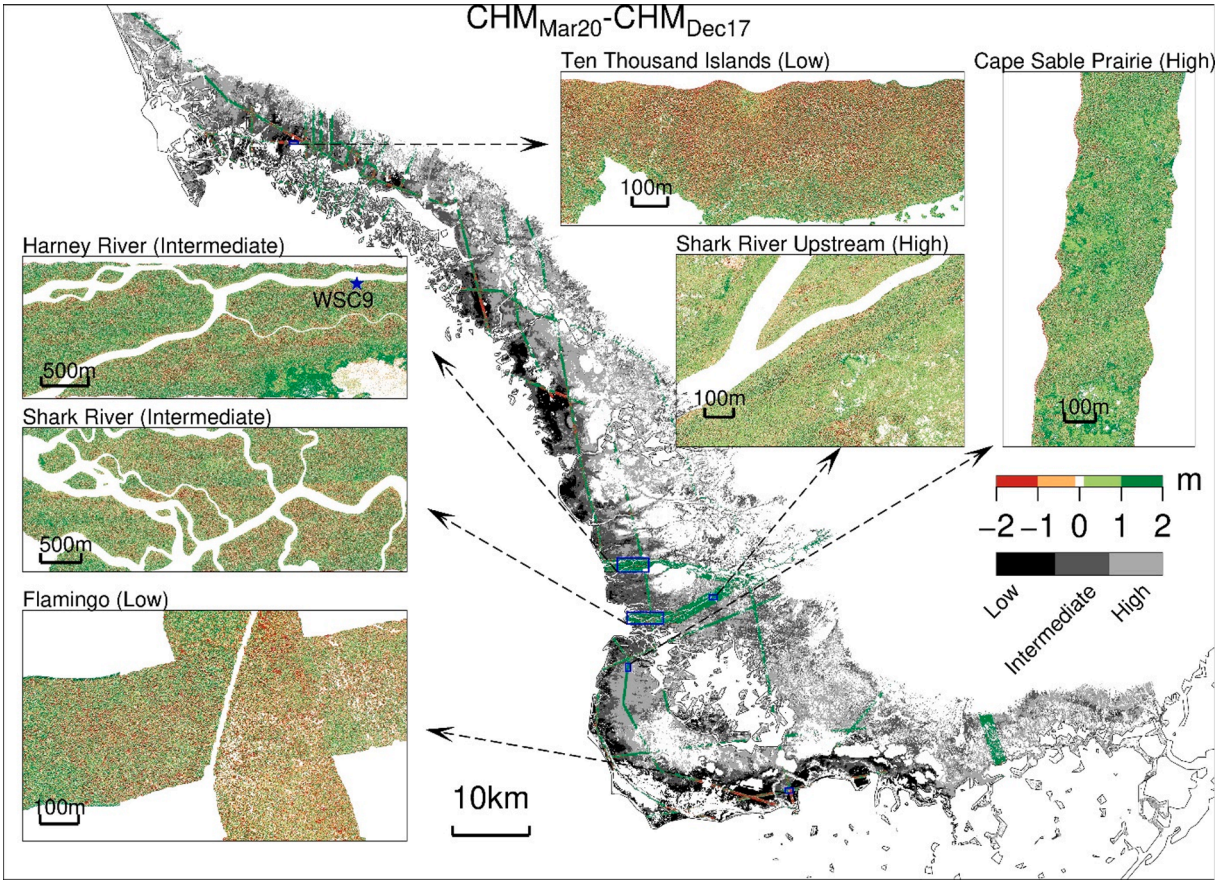

Fig. 4. Canopy height regrowth of mangrove forests in South Florida from December 2017 to March 2020 show patterns that track with previous satellite observations from Lagomasino et al. (2021). Areas of green show increases in mangrove canopy after Hurricane Irma, while areas in orange/red indicate areas of additional mangrove canopy height loss. (For interpretation of the references to color in this figure legend, the reader is referred to the web version of this article.)

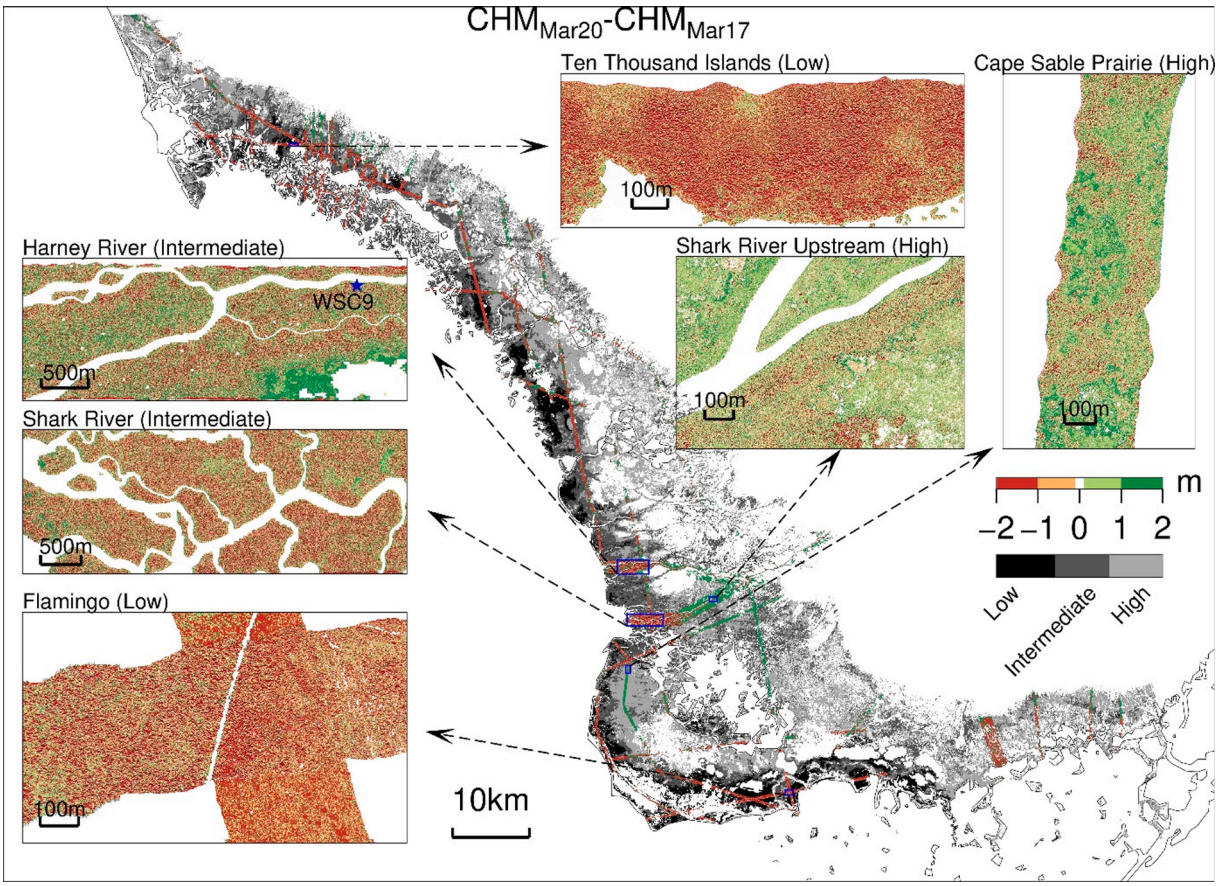

Fig. 5. The spatial distribution of canopy height recovery of mangrove forests in South Florida from March 2017 to March 2020 indicate a wide range of responses to Hurricane Irma.

Table 1
The regrowth rate and recover rate of mangrove forests in South Florida show large differences between resilience class types. The regrowth rate is the ratio of the number of pixels that have positive change over the total number of pixels in CHMs from March 2020 to December 2017. The recovery rate is the ratio of the number of pixels that have a positive change over the total number of pixels in CHMs from March 2020 to March 2017. CHMs were resampled to 30 m before calculation.

Resilience class	Regrowth rate (CHM_{Mar20} - CHM_{Dec17})	Recover rate (CHM_{Mar20} - $CHM_{March17}$)
Low	49.2 %	9.6 %
Intermediate	85.0 %	30.2 %
High	95.1 %	57.5 %
Total	84.7 %	38.1 %

to 31.2 %) while the density of mangroves below 5 m increased from 31.5 % to 39.6 % (Fig. 6b). These changes in the canopy structure were significantly different before and after Hurricane Irma according to the two-sided Kolmogorov–Smirnov (KS) test, but only for the low and intermediate resilience categories (Table 2). The canopy height distribution did not change significantly after 2.5 years of growth, between CHM_{Dec17} and CHM_{Mar20}, for both low and intermediate resilience classes as noted by the KS test.

Mangrove forests within the high resilience class experienced the least amount of canopy structure change compared to pre-Irma conditions (Fig. 6c). In these areas, mangroves are dominated by shorter canopies (<5 m) and are generally located at the inland mangrove boundary that can be up to 25 km upstream of estuaries from the Gulf of Mexico. These short stature mangroves exhibited minimal change across the three time periods, whereas there was a modest change in canopy height where tall mangroves (>15 m) occur in this region, though not statistically different as measured by the KS test (Table 2).

3.2. Canopy structural changes by different height classes

Hurricane Irma caused long-lasting and significant damages to mangrove forest structure in ENP. Overall, the mean canopy height decreased 0.72 m for mangroves scanned by G-LiHT in the three months after Irma but only recovered by 0.1 m in the 2.5 years following the storm (Table 3). Approximately 77.0 % of the surveyed area experienced canopy height loss three months after Hurricane Irma. The magnitude of canopy shortening is correlated with canopy height, whereby taller forests experienced more damage and more recovery than shorter ones (Table 3). For mangrove forests that were above 10 m, the average canopy height loss exceeded 2 m. The larger magnitude changes in canopy height were observed in mangrove areas close to the mouth of Shark and Harney River estuaries, where the tallest mangroves are located in the study area.

In the 2.5 years after Hurricane Irma, most of the mangrove forests (84.7 % of the survey area) experienced canopy height regrowth. However, the mean canopy height only increased by 0.10 m. We identified similar canopy height dependent patterns, whereby forested areas with taller mangroves experienced more growth than shorter forests. The average regrowth for pre-storm canopy height over 15 m, was ~ 1 m, and progressively reduced with decreasing canopy height (Table 3). For each canopy height class from short to tall, the amount of regrowth for each height class following the storm restored from 17 to 35 % of the canopy height lost by Hurricane Irma. In fact, only 38.1 % of the survey area has recovered to pre-storm canopy height, the majority of which occurred in areas that received little to no damage.

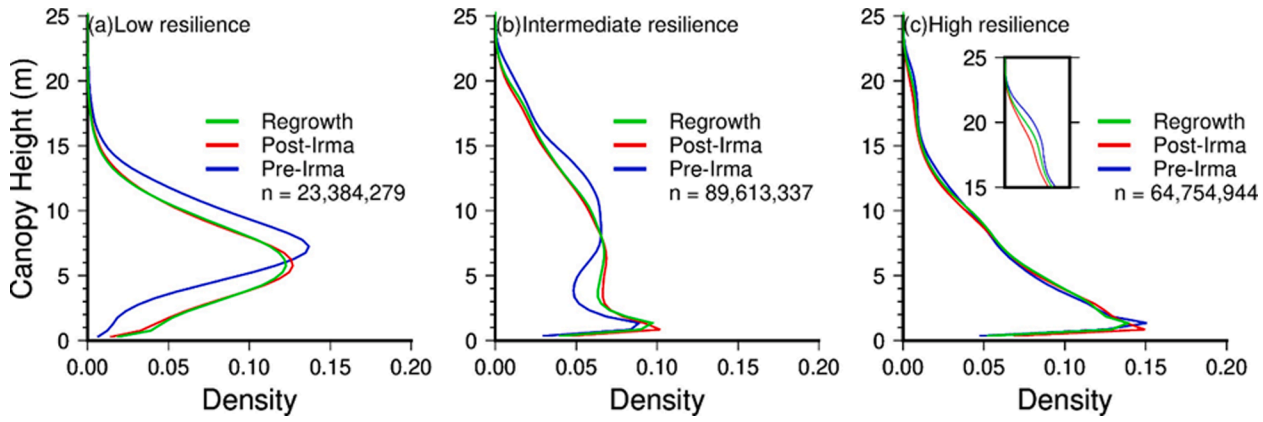

Fig. 6. Density plots of canopy height from G-LiHT derived CHMs in low (a), intermediate (b), and high (c) resilience classes. The binwidth for the density distribution is 0.5 m. The "n" value is equal to the number of 1 m by 1 m pixels within the CHM.

Table 2
Two-sided Kolmogorov-Smirnov statistics (KS), critical KS statistics (KScrit), and *p* value for each resilience class. We randomly sampled 500 points in each resilience class and determine whether distributions between Pre-Irma (March 2017), Post-Irma (Dec 2017), and Regrowth (March 2020) were significant.

Resilience class	Group	KS	KScrit	*P*-value
High	Pre-Post	0.072	0.061	0.15
	Pre-Regrowth	0.030	0.061	0.98
	Post-Regrowth	0.060	0.061	0.33
Intermediate	Pre-Post	0.120	0.061	<0.01
	Pre-Regrowth	0.144	0.061	<0.01
	Post-Regrowth	0.042	0.061	0.77
Low	Pre-Post	0.192	0.061	<0.01
	Pre-Regrowth	0.228	0.061	<0.01
	Post-Regrowth	0.068	0.061	0.20

3.3. Canopy structural changes by different species classes

Mangrove canopy height and recovery also varied by species composition. The accurate mangrove species map of region 1–4 in ENP was identified by photo-interpreters over stereoscopic color infrared aerial imagery and each cell represented the dominant community (Ruiz et al., 2021). On average, tree height of *R. mangle* and *C. erectus* dominated forests were the shortest, with the majority of their canopy height being less than 5 m tall (Fig. 7). The average canopy heights for the remaining classes range between 7 and 10 m. Tall mangroves were mainly found in mixed forests and *L. racemosa* dominated areas, and they can reach up to ~ 25 m near the mouth of Shark River. The distribution of canopy height for each species cover class were compared by performing a Tukey HSD Test among the five dominated vegetation cover classes in March 2017 (Table 4). Nearly all the adjusted *p*-values of "*p* adj" in group comparison are less than 0.05. We can conclude that these five vegetation groups are significantly different at the 95th percent confidence level.

The change in mangrove canopy following Hurricane Irma also varied by species. On average, the CHM_{Dec17} of *R. mangle* decreased only 0.19 m after Irma (Table 5). After 2.5 years, the CHM_{Mar20} of *R. mangle* was still below pre-storm height, however, there was no significant difference between time periods as recorded by the KS test between the distribution of pre-, post-Irma and after regrowth (Table 6). *A. germinans* were significantly ($p < 0.01$) shortened by 1.10 m after Irma and exhibited the lowest regrowth rate (2.54 % after 2.5 years), calculated as the ratio of average regrowth height to the average canopy height post-Irma (December 2017). This low rate of recovery had no significant effect on the canopy height distribution between CHM_{Dec17} and CHM_{Mar20}. *L. racemosa* also experienced severe damage after Irma, but for this species, the growth rate was the highest among all mangrove species, at 8.75 %, and showed a significant difference between each time prior (Fig. 7; Table 6). The canopy height of *C. erectus* had a similar range as *R. mangle* (Fig. 7), but this species exhibited a damage rate of 11.7 %, which was nearly 3 times larger than that of *R. mangle* (Table 5). Similarly, the regrowth rate was 6.62 %, which was substantially higher recover rate than *R. mangle*. For mixed mangroves, we observed the highest damage rate (-15.75 %) due to Irma and the regrowth is 0.68 m on average (Table 5).

4. Discussion

4.1. Canopy restructuring following Hurricane Irma

Canopy height models (CHMs) derived from the G-LiHT data showed that the tallest mangroves (>20 m) are still primarily concentrated around the mouth of Shark River estuary in the southwest coast of ENP, corresponding to previous studies (Simard et al., 2006; E. A. Feliciano et al., 2017). We show that high resolution CHMs from multiple lidar data can be used to verify the recovery patterns of mangrove forests

Table 3
The statistics of average canopy height per time period from G-LiHT data show patterns that are related to the original canopy height. Damage in meters indicates the average canopy height change between pre-(Mar 2017) and post-Irma (Dec 2017). Damage in percentages is the ratio of change to the average canopy height pre-Irma. Regrowth in meters indicates the average canopy height change between post-Irma (Dec 2017) and regrowth (March 2020). Regrowth in percentages is the ratio of change to the average canopy height post-Irma (Dec 2017).

	Mar 2017		Dec 2017		Mar 2020		Damage		Regrowth	
	Mean (m)	Std (m)	Mean (m)	Std (m)	Mean (m)	Std (m)	(m)	(%)	(m)	(%)
>20	20.56	2.36	16.23	6.35	17.25	5.52	−4.33	−21.06 %	1.02	6.28 %
15–20	16.90	2.69	14.08	5.14	15.06	4.65	−2.82	−16.69 %	0.98	6.96 %
10–15	12.05	2.72	10.04	3.92	10.38	3.86	−2.01	−16.68 %	0.34	3.39 %
5–10	7.43	2.53	6.59	2.72	6.76	2.78	−0.84	−11.31 %	0.17	2.58 %
0–5	2.56	2.07	2.49	2.07	2.54	5.06	−0.07	−2.73 %	0.05	2.01 %
Total	7.22	5.23	6.50	4.80	6.60	5.01	−0.72	−9.97 %	0.10	1.54 %

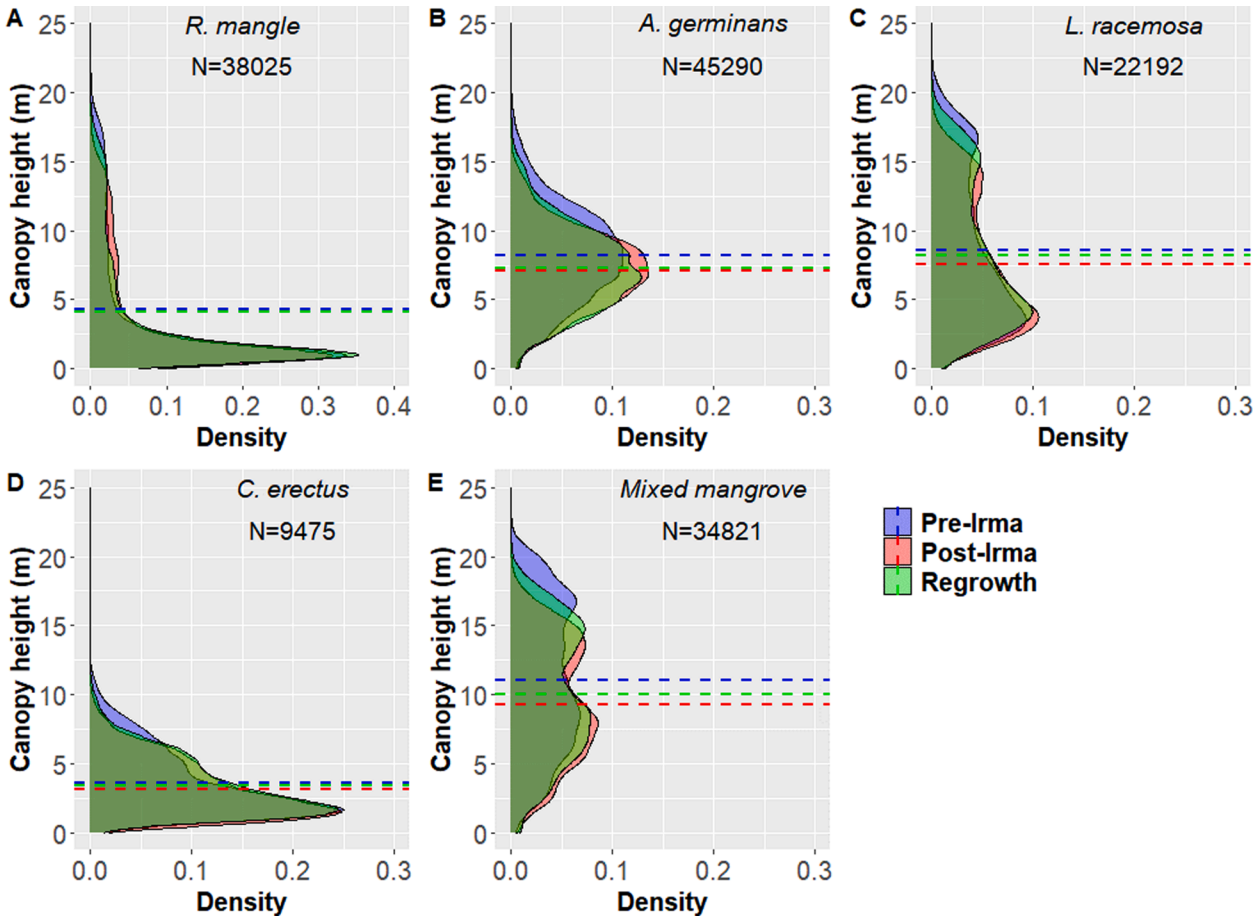

Fig. 7. Density plots of canopy height in five dominant mangrove vegetation classes (*R. mangle, A. germinans*, *L. racemosa*, *C. erectus*, and mixed mangroves) show distinct species-specific patterns. Pre-Irma, Post-Irma, and Regrowth correspond to March 2017, Dec 2017, and March 2020, respectively. Value of 'n' represents the number of pixels (30 m) from CHMs in each species. Blue, red, and green dashed lines represent mean canopy height in each dominant mangrove species class in pre-Irma, post-Irma, and regrowth periods, respectively. (For interpretation of the references to color in this figure legend, the reader is referred to the web version of this article.)

Table 4
Tukey HSD test results between the five dominated mangrove species (*A. germinans*, *L. racemosa*, *R. mangle*, *C. erectus*, and Mixed mangroves) in March 2017 indicate significant differences between species types. In each class, we randomly selected 5,00 sample points from the CHMs.

Group	Diff	*P*-value
C. erectus-A. germinans	−4.65	0
Mixed mangroves-*A. germinans*	2.77	0
R. mangle-A. germinans	−4.09	0
L. racemosa -A. germinans	0.30	<0.01
Mixed mangroves-*C. erectus*	7.42	0
R. mangle-C. erectus	0.56	0
L. racemosa -C. erectus	4.96	0
R. mangle-Mixed mangroves	−6.86	0
L. racemosa -Mixed mangroves	−2.46	0
L. racemosa -R. mangle	4.39	0

predicted by short-term satellite-based resilience models (e.g., derived within 1 year after the hurricane). Mangroves in high resilience class (e.g., upstream of the Shark River, Cape Sable Prairie) showed quick recovery within 2.5 years. However, the canopy structure damaged by Hurricane Irma in low (e.g., Cape Sable/Flamingo) and intermediate (e.g., downstream Shark and Harney Rivers) resilience classes showed little or no change in their distribution and neither has recovered to pre-storm levels, indicating that the canopy recovery process can take multiple years (Fig. 5 and Fig. 6). Growth stalls in low resilience class due to the high mortality rates of mangrove trees and the lack of regeneration and recruitment of new individuals. In fact, massive die backs occurred in low resilience class after Hurricane Irma, especially near Gopher Key and Cape Stable (Lagomasino et al., 2021).

The spatial and temporal recovery patterns of mangroves are influenced by pre-storm initial forest structural conditions (e.g., canopy height, canopy gaps, and fractional vegetation cover), rates of sapling

Table 5
Statistics of canopy height changes for each mangrove species after Hurricane Irma indicate species-specific recovery patterns following the hurricane.

Dominant mangrove species	Mar 2017		Dec 2017		Mar 2020		Damage		Regrowth	
	Mean (m)	Std (m)	Mean (m)	Std (m)	Mean (m)	Std (m)	(m)	(%)	(m)	(%)
R. mangle	4.34	4.98	4.15	4.24	4.11	4.46	−0.19	−4.38 %	−0.04	−0.96 %
A. germinans	8.2	3.46	7.1	2.83	7.28	3.06	−1.1	−13.41 %	0.18	2.54 %
L. racemosa	8.59	5.35	7.54	4.51	8.2	4.93	−1.05	−12.22 %	0.66	8.75 %
C. erectus	3.59	2.34	3.17	1.98	3.38	2.04	−0.42	−11.70 %	0.21	6.62 %
Mixed mangroves	11.05	5.18	9.31	4.28	9.99	4.6	−1.74	−15.75 %	0.68	7.30 %

Table 6
Two-sided Kolmogorov-Smirnov statistics (KS), critical KS statistics (KScrit), and *p* value for dominated vegetation cover classes. We randomly sampled 500 points in each class and determine whether distributions between Pre-Irma (March 2017), Post-Irma (Dec 2017), and Regrowth (March 2020) were significant.

Dominant mangrove species	Group	KS	Kscrit	*P*-value
R. mangle	Pre-Post	0.070	0.061	0.17
	Pre-Regrowth	0.046	0.061	0.67
	Post-Regrowth	0.050	0.061	0.56
A. germinans	Pre-Post	0.208	0.061	<0.01
	Pre-Regrowth	0.148	0.061	<0.01
	Post-Regrowth	0.074	0.061	0.13
L. racemosa	Pre-Post	0.148	0.061	<0.01
	Pre-Regrowth	0.090	0.061	0.03
	Post-Regrowth	0.098	0.061	0.02
C. erectus	Pre-Post	0.110	0.061	<0.01
	Pre-Regrowth	0.096	0.061	0.02
	Post-Regrowth	0.052	0.061	0.51
Mixed mangroves	Pre-Post	0.174	0.061	<0.01
	Pre-Regrowth	0.110	0.061	<0.01
	Post-Regrowth	0.126	0.061	<0.01

recruitment, species composition, and environmental attributes such as topography, tidal connectivity, and sea level rise (Twilley and Chen, 1998; Asbridge et al., 2018; Rivera-Monroy et al., 2019; Krauss and Osland, 2020; Lagomasino et al., 2021; Peereman et al., 2022). As other studies have noted, taller mangroves tend to suffer more height loss than shorter mangroves because they are more susceptible to breakage or uprooting due to strong winds (Roth, 1992; Smith et al., 1994; Aung et al., 2013; Taillie et al., 2020). The regrowth rate was also higher in taller forests, particularly in near-coast mangrove areas. The tidal connectivity in these regions helped to limit stagnant ponding and reduce the effects of hyper salinization and sulfide build-up in the soil (Lagomasino et al., 2021). In addition, P-rich mineral sediments deposited by hurricanes to near-coast mangroves, particularly in the southwestern Everglades, enhance P concentrations in the soil, increase plant uptake, stimulate soil peat development, and facilitate rapid forest recovery (Castañeda-Moya et al., 2010, 2020).

We also quantify the recovery of mangroves based on the pre-hurricane species composition. Forests dominated by *R. mangle* shows little change in canopy height following Hurricane Irma. This is a result of the short canopy stature that minimizes the impact from strong winds as well as *R. mangle* forests are generally found further inland and far away from the most severe storm impacts. The short structure allows for this species to avoid stem damage as it will not survive if the stems are snapped or damaged because they lack vegetative reproduction (i.e., epicormic growth) and cannot resprout (Smith et al., 2009). *A. germinans* showed significant damages after Hurricane Irma, and are generally located in low-lying and disconnected areas (Lagomasino et al., 2021). Here, the regrowth rate was minimal and there was no difference in the distribution of canopy height post-Irma. This has further confirmed the extensive dieback of *A. germinans* following Hurricane Irma. In the case of *L. racemosa*, previous studies suggested this species can have more structural damage than *R. mangle* (Baldwin et al., 1995, 2001), however we found higher recovery rates for *L. racemosa* which could be associated with the species ability to resprout from the stem (Baldwin et al., 2001; Milbrandt et al., 2006). Indeed, previous studies in the study area have reported the faster recovery rate of this species in the mid- and downstream regions of Shark River estuary following Hurricane Wilma (Rivera-Monroy et al., 2019). This is associated to the physiological adaptations and traits of this species (e.g., shade intolerance, high photosynthesis rates, epicormic growth; (Twilley and Chen, 1998)) and the ability of this species to dominate in mangrove areas where canopy gaps are created as a result of lightning strikes, mortality, or massive defoliation during hurricanes (Roth, 1992; Chen and Twilley, 1999; Zhang et al., 2008; Rivera-Monroy et al., 2019). The interaction between canopy gap dynamics and species traits and tolerance will largely control the magnitude and rate of mangrove recovery and change following disturbance (Twilley and Chen, 1998; Lugo, 2008; Shiels et al., 2015; Rivera-Monroy et al., 2019).

4.2. Challenges, needs, and future impacts to mangrove forests

One challenge is to distinguish the lateral and vertical changes of mangroves from Canopy Height Models. Possible constrains could be a threshold of maximum vertical height growth and horizontal extent of mangrove crowns, as applied in a forest recovery study following Hurricane Maria (Leitold et al., 2021). New seedlings and saplings could regenerate and recruit into juvenile adult cohorts through canopy gaps and patches created by hurricanes, contributing to increases in stem density and basal area post-disturbance. Previous studies also used airborne lidar to quantify the canopy gaps after hurricane disturbances (Zhang, 2008; Zhang et al., 2008). Changes in canopy gaps are important for quantifying mangrove forest turnover and successional patterns of mangrove species. Further study for quantifying these gaps following Hurricane Irma should be investigated. The combination of airborne lidar and satellite data such as Landsat, TanDEM-X could be used to map the whole mangrove area in South Florida (E. A. Feliciano et al., 2017). Despite these limitations, repeated airborne lidar survey for mangrove disturbances study pave the way for repeated spaceborne lidar survey such as GEDI and ICESat-2 at a large scale.

Accuracy analyses of CHMs from G-LiHT lidar point cloud, resilience maps, and dominant mangrove species maps are strongly needed. Accuracy of CHMs is critical in our interpretation of canopy changes. The vertical accuracy of ground elevation by airborne lidar can range from 10 ~ 30 cm, depending on terrain slopes and vegetations density (Xiong et al., 2018). The accuracy of lidar measurements is also largely dominated by accuracy of GNSS instruments (Xiong et al., 2019). The accuracy of DEM and DSMs in this study were about ~ 10 cm, which is similar to the accuracy of GNSS solutions. This could be verified by comparisons between concrete road surfaces during the three repeated lidar surveys. In addition, the Canopy Height Model (CHM) is the relative difference between DSM and DEM. The systematic GNSS error can be cancelled out and it is much more accurate. G-LiHT can detect changes of mangrove canopy height that are larger than ~ 10 cm for each measurement. In Fig. 4 and Fig. 5, we do show mangrove canopy height regrowth and recovery for overlapping pixels by differencing the CHMs. The accuracy of resilience maps, species maps may have larger impacts on growth changes on a per pixel basis. However, we focus on canopy height frequency distribution changes on at large scale in these sections. Our overall regrowth represents the mean canopy height change over the entire class, but each class includes thousands of canopy height pixels (1 m by 1 m). The small changes in the overall mean height could suggest a significant shift of the canopy structure (Table 2, 4, and 6).

Mangrove forest structural attributes, especially canopy height and basal area, are important metrics to quantify aboveground biomass and carbon stocks (Simard et al., 2019). The tallest mangroves are found mainly in the wettest and hottest regions with low cyclone frequency, low soil salinity, and low human population. In fact, 74 % of global mangrove canopy height can be explained by precipitation, temperature, and cyclone frequency (Simard et al., 2019). Although mangrove forests are resilient and disturbance-adapted ecosystems, increased frequency of cyclones may restrict the growth of mangrove forests and reduce mangrove structural complexity (Lugo and Snedaker, 1974; Simard et al., 2019). Mangrove forests could also become more resistant to canopy damages with more frequent cyclones (Peereman et al., 2022) but may result in shorter mangrove forests, and subsequent decrease in carbon stocks. In the Caribbean region, cyclone frequency is projected to increase into the future as a result of climate change (Mendelsohn et al., 2012; Kossin et al., 2020). Our results show only 38.1 % of mangrove forests canopy height have recovered to pre-storm levels 2.5 years after

Hurricane Irma. Based on these recovery times after cyclones, mangrove forest structure could be permanently altered if additional cyclones hit South Florida while the mangroves are not fully recovered (Peereman et al., 2022). Nearly all ecosystem services that mangrove provide would also be affected, especially reducing the ability of carbon sequestration and coastal protection. Accumulated cyclone effects could cause increased mangrove forest mortality, or even peat collapse. In this case, mangrove ecosystem could be converted to open water pond or mudflat (Osland et al., 2020).

5. Conclusion

Mangroves in South Florida have been impacted by numerous hurricanes and freeze events which have drastically altered the extent, and the structure and function of the forests in this region (Baldwin et al., 1995; Smith et al., 2009; Danielson et al., 2017; Rivera-Monroy et al., 2019; Osland et al., 2020; Radabaugh et al., 2020; Lagomasino et al., 2021). Quantifying the structural changes caused by these pulsing events are critical for understanding the disturbance dynamics, particularly for quantifying resistance, resilience, and trajectories of recovery of mangrove forests. In this study we focus on the recovery and regrowth of mangrove forests in South Florida following Hurricane Irma. Hurricane Irma caused remarkable damages to mangrove forests in South Florida that have imprinted a new legacy on the forest that continues 2.5 years later. This Irma footprint, and now legacy imprint on the mangrove forests was captured and well-documented by repeated NASA G-LiHT lidar surveys. Canopy structures show variable patterns among different resilience, height, and species classes. In low and intermediate classes, canopy structure was not recovering even after 2.5 years following Irma, although regrowth is detected over mangrove forests. Tall mangroves suffered more loss but recovered faster than short stature mangroves. We also found *L. racemosa* that experienced the most severe damage but was followed by the fastest regrowth rate of all five mangrove species classes tested. The recovery process of mangrove forests in South Florida is still ongoing, but with some areas showing a clear decline and the potential for a rapid transformation in habitat conditions. Long term and regular lidar surveys for coastal ecosystem monitoring are needed to identify vulnerable mangroves, especially in low-lying regions and to mitigate the hurricane impacts by human efforts. Resilience of mangrove forests will also be significantly affected by the increase of the frequency and magnitude of hurricanes due to climate change (Goldberg et al., 2020). Developing accurate coastal ecosystem models will be important for coastal managers to reduce coastal vulnerability and prepare for future hurricanes.

CRediT authorship contribution statement

Lin Xiong: Methodology, Writing – original draft, Writing – review & editing. **David Lagomasino:** Conceptualization, Supervision, Methodology, Writing – review & editing. **Sean P. Charles:** Writing – review & editing. **Edward Castañeda-Moya:** Writing – review & editing. **Bruce D. Cook:** Validation, Resources, Software. **Jed Redwine:** Writing – review & editing. **Lola Fatoyinbo:** Supervision, Resources, Writing – review & editing.

Declaration of Competing Interest

The authors declare that they have no known competing financial interests or personal relationships that could have appeared to influence the work reported in this paper.

Data availability

Data will be made available on request.

Acknowledgments

The authors thank the editor and reviewers for providing valuable suggestions and comments on the manuscript. The authors also thank the ENP for granting research permits to conduct G-LiHT airborne campaigns in South Florida. All figures are prepared using the Generic Mapping Tools (GMT), which is free and open-source software to the academic community (https://www.generic-mapping-tools.org/). This study is funded by NASA program no. 80NSSC18K0163 and 80NSSC20K1120, as well as the Interagency Climate Change NASA program grant no. 2017-67003-26482/project accession no. 1012260 from the USDA National Institute of Food and Agriculture. The Florida Coastal Everglades Long-Term Ecological Research (FCE-LTER) program funded by the National Science Foundation (Grant #DEB-2025954) provided partial funding for E.C-M. This is publication #1490 from the Institute of Environment at Florida International University.

References

Abhik, S., Hope, P., Hendon, H.H., Hutley, L.B., Johnson, S., Drosdowsky, W., Brown, J. R., Duke, N.C., 2021. Influence of the 2015–2016 El Niño on the record-breaking mangrove dieback along northern Australia coast. Sci. Rep. 11 (1), 1–12.

Abtew, W., Huebner, R.S., Ciuca, V., 2005. Chapter 5: Hydrology of the South Florida Environment. 2006 South Florida Environmental Report, G. Redfield (Ed.).

Alongi, D.M., 2020. Carbon balance in salt marsh and mangrove ecosystems: A global synthesis. J. Mar. Sci. Eng. 8 (10), 767.

Andersen, H.E., Reutebuch, S.E., McGaughey, R.J., d'Oliveira, M.V.N., Keller, M., 2014. Monitoring selective logging in western amazonia with repeat lidar flights. Remote Sens. Environ. 151, 157–165.

Asbridge, E., Lucas, R., Rogers, K., Accad, A., 2018. The extent of mangrove change and potential for recovery following severe Tropical Cyclone Yasi, Hinchinbrook Island, Queensland, Australia. Ecol. Evolut. 8 (21), 10416–10434.

Aung, T.T., Mochida, Y., Than, M.M., 2013. Prediction of recovery pathways of cyclone-disturbed mangroves in the mega delta of Myanmar. For. Ecol. Manage. 293, 103–113.

Baldwin, A., Platt, W.J., Gathen, K.L., Lessmann, J.M., Rauch, T.J., 1995. Hurricane damage and regeneration in fringe mangrove forests of southeast Florida, USA. J. Coastal Res. 169–183.

Baldwin, A., Egnotovich, M., Ford, M., Platt, W., 2001. Regeneration in Fringe Mangrove Forests Damaged. Plant Ecol. 157 (2), 151–164.

Barr, J.G., Engel, V., Smith, T.J., Fuentes, J.D., 2012. Hurricane disturbance and recovery of energy balance, CO 2 fluxes and canopy structure in a mangrove forest of the Florida Everglades. Agric. For. Meteorol. 153, 54–66.

Bouillon, S., Borges, A. V, Castañeda-Moya, E., Diele, K., Dittmar, T., Duke, N. C., Kristensen, E., Lee, S. Y., Marchand, C., Middelburg, J. J., others., 2008. Mangrove production and carbon sinks: a revision of global budget estimates. Global Biogeochem. Cycles 22(2).

Cahoon, D.R., Hensel, P., Rybczyk, J., McKee, K.L., Proffitt, C.E., Perez, B.C., 2003. Mass tree mortality leads to mangrove peat collapse at Bay Islands, Honduras after Hurricane Mitch. J. Ecol. 91 (6), 1093–1105.

Cangialosi, J.P., Latto, A.S., Berg, R., 2018. Hurricane Irma (AL112017): 30 August–12 September 2017. National Hurricane Center Tropical Cyclone Report, 111.

Castañeda-Moya, E., Twilley, R.R., Rivera-Monroy, V.H., Zhang, K., Davis, S.E., Ross, M., 2010. Sediment and nutrient deposition associated with Hurricane Wilma in mangroves of the Florida Coastal Everglades. Estuaries Coasts 33 (1), 45–58.

Castañeda-Moya, E., Twilley, R.R., Rivera-Monroy, V.H., 2013. Allocation of biomass and net primary productivity of mangrove forests along environmental gradients in the Florida Coastal Everglades, USA. For. Ecol. Manage. 307, 226–241.

Castañeda-Moya, E., Rivera-Monroy, V.H., Chambers, R.M., Zhao, X., Lamb-Wotton, L., Gorsky, A., Gaiser, E.E., Troxler, T.G., Kominoski, J.S., Hiatt, M., 2020. Hurricanes fertilize mangrove forests in the Gulf of Mexico (Florida Everglades, USA). Proc. Natl. Acad. Sci. USA 117 (9), 4831–4841.

Ceron, C.N., Melesse, A.M., Price, R., Dessu, S.B., Kandel, H.P., 2015. Operational actual wetland evapotranspiration estimation for South Florida using MODIS imagery. Remote Sens. 7 (4), 3613–3632.

Charles, S., Lagomasino, D., Payton, A., 2021. Mangrove expansion exceeds loss across South Florida despite major storm damage in the last 38 years. AGU Fall Meeting 2021.

Chen, R., Twilley, R.R., 1999. A simulation model of organic matter and nutrient accumulation in mangrove wetland soils. Biogeochemistry 44 (1), 93–118.

Cook, B.D., Corp, L.A., Nelson, R.F., Middleton, E.M., Morton, D.C., McCorkel, J.T., Masek, J.G., Ranson, K.J., Ly, V., Montesano, P.M., 2013. NASA goddard's LiDAR, hyperspectral and thermal (G-LiHT) airborne imager. Remote Sens. 5 (8), 4045–4066.

Dalponte, M., Jucker, T., Liu, S., Frizzera, L., Gianelle, D., 2019. Characterizing forest carbon dynamics using multi-temporal lidar data. Remote Sens. Environ. 224, 412–420.

Danielson, T.M., Rivera-Monroy, V.H., Castañeda-Moya, E., Briceño, H., Travieso, R., Marx, B.D., Gaiser, E., Farfán, L.M., 2017. Assessment of Everglades mangrove forest

resilience: Implications for above-ground net primary productivity and carbon dynamics. For. Ecol. Manage. 404, 115–125.
Del Valle, A., Eriksson, M., Ishizawa, O.A., Miranda, J.J., 2020. Mangroves protect coastal economic activity from hurricanes. Proc. Natl. Acad. Sci. 117 (1), 265–270.
Dessu, S.B., Price, R.M., Troxler, T.G., Kominoski, J.S., 2018. Effects of sea-level rise and freshwater management on long-term water levels and water quality in the Florida Coastal Everglades. J. Environ. Manage. 211, 164–176.
Donato, D.C., Kauffman, J.B., Murdiyarso, D., Kurnianto, S., Stidham, M., Kanninen, M., 2011. Mangroves among the most carbon-rich forests in the tropics. Nat. Geosci. 4 (5), 293–297.
Drake, J.B., Dubayah, R.O., Clark, D.B., Knox, R.G., Blair, J.B., Hofton, M.A., Chazdon, R. L., Weishampel, J.F., Prince, S., 2002. Estimation of tropical forest structural characteristics using large-footprint lidar. Remote Sens. Environ. 79 (2–3), 305–319.
Dubayah, R.O., Drake, J.B., 2000. Lidar remote sensing for forestry. J. Forest. 98 (6), 44–46.
Duever, M.J., Meeder, J.F., Meeder, L.C., McCollom, J.M., 1994. The climate of south Florida and its role in shaping the Everglades ecosystem. The Ecosystem and Its Restoration, Everglades, pp. 225–248.
Duke, N.C., Kovacs, J.M., Griffiths, A.D., Preece, L., Hill, D.J.E., Van Oosterzee, P., Mackenzie, J., Morning, H.S., Burrows, D., 2017. Large-scale dieback of mangroves in Australia's Gulf of Carpentaria: a severe ecosystem response, coincidental with an unusually extreme weather event. Mar. Freshw. Res. 68 (10), 1816–1829.
Fatoyinbo, T., Feliciano, E.A., Lagomasino, D., Lee, S.K., Trettin, C., 2018. Estimating mangrove aboveground biomass from airborne LiDAR data: A case study from the Zambezi River delta. Environ. Res. Lett. 13 (2).
Feliciano, E.A., Wdowinski, S., Potts, M.D., Lee, S.K., Fatoyinbo, T.E., 2017. Estimating mangrove canopy height and above-ground biomass in the Everglades National Park with airborne LiDAR and TanDEM-X data. Remote Sens. 9 (7).
Feliciano, E., 2015. Multi-Scale Remote Sensing Assessments of Forested Wetlands: Applications to the Everglades National Park.
Friess, D.A., Rogers, K., Lovelock, C.E., Krauss, K.W., Hamilton, S.E., Lee, S.Y., Lucas, R., Primavera, J., Rajkaran, A., Shi, S., 2019. The state of the world's mangrove forests: past, present, and future. Annu. Rev. Environ. Resour. 44, 89–115.
Gedan, K.B., Kirwan, M.L., Wolanski, E., Barbier, E.B., Silliman, B.R., 2011. The present and future role of coastal wetland vegetation in protecting shorelines: answering recent challenges to the paradigm. Clim. Change 106 (1), 7–29.
Goldberg, L., Lagomasino, D., Thomas, N., Fatoyinbo, T., 2020. Global declines in human-driven mangrove loss. Glob. Change Biol. 26 (10), 5844–5855.
Han, X., Feng, L., Hu, C., Kramer, P., 2018. Hurricane-Induced Changes in the Everglades National Park Mangrove Forest: Landsat Observations Between 1985 and 2017. J. Geophys. Res. Biogeosci. 123 (11), 3470–3488.
Heumann, B.W., 2011. Satellite remote sensing of mangrove forests: Recent advances and future opportunities. Prog. Phys. Geogr. 35 (1), 87–108.
Hudak, A.T., Strand, E.K., Vierling, L.A., Byrne, J.C., Eitel, J.U.H., Martinuzzi, S., Falkowski, M.J., 2012. Quantifying aboveground forest carbon pools and fluxes from repeat LiDAR surveys. Remote Sens. Environ. 123, 25–40.
Imbert, D., 2018. Hurricane disturbance and forest dynamics in east Caribbean mangroves. Ecosphere 9 (7).
Jennerjahn, T.C., Ittekkot, V., 2002. Relevance of mangroves for the production and deposition of organic matter along tropical continental margins. Naturwissenschaften 89 (1), 23–30.
Keim, B.D., Muller, R.A., Stone, G.W., 2007. Spatiotemporal patterns and return periods of tropical storm and hurricane strikes from Texas to Maine. J. Clim. 20 (14), 3498–3509.
Kossin, J.P., Knapp, K.R., Olander, T.L., Velden, C.S., 2020. Global increase in major tropical cyclone exceedance probability over the past four decades. Proc. Natl. Acad. Sci. 117 (22), 11975–11980.
Kovacs, J.M., Wang, J., Blanco-Correa, M., 2001. Mapping disturbances in a mangrove forest using multi-date Landsat TM imagery. Environ. Manage. 27 (5), 763–776.
Krauss, K.W., Osland, M.J., 2020. Tropical cyclones and the organization of mangrove forests: A review. Ann. Bot. 125 (2), 213–234.
Kronseder, K., Ballhorn, U., Böhm, V., Siegert, F., 2012. Above ground biomass estimation across forest types at different degradation levels in Central Kalimantan using LiDAR data. Int. J. Appl. Earth Obs. Geoinf. 18, 37–48.
Kuenzer, C., Bluemel, A., Gebhardt, S., Quoc, T. V., Dech, S., 2011. Remote sensing of mangrove ecosystems: A review. In: Remote Sensing (Vol. 3, Issue 5). Molecular Diversity Preservation International.
Lagomasino, D., Price, R.M., Whitman, D., Melesse, A., Oberbauer, S.F., 2015. Spatial and temporal variability in spectral-based surface energy evapotranspiration measured from Landsat 5TM across two mangrove ecotones. Agric. For. Meteorol. 213, 304–316.
Lagomasino, D., Fatoyinbo, L., Castaneda, E., Cook, B., Montesano, P., Neigh, C., Corp, L., Ott, L., Chavez, S., Morton, D., 2021. Storm surge and ponding explain mangrove dieback in southwest Florida following Hurricane Irma. Nat. Commun.
Lee, Duncan, C., Nicholson, E., Fatoyinbo, T. E., Lagomasino, D., Thomas, N., Worthington, T.A., Murray, N.J., 2021. Mapping the extent of mangrove ecosystem degradation by integrating an ecological conceptual model with satellite data. Remote Sens. 13(11), 1–19.
Lee, S.Y., Primavera, J.H., Dahdouh-Guebas, F., McKee, K., Bosire, J.O., Cannicci, S., Diele, K., Fromard, F., Koedam, N., Marchand, C., et al., 2014. Ecological role and services of tropical mangrove ecosystems: a reassessment. Glob. Ecol. Biogeogr. 23 (7), 726–743.
Lefsky, M.A., Cohen, W.B., Parker, G.G., Harding, D.J., 2002. Lidar remote sensing for ecosystem studies. Bioscience 52 (1), 19–30.
Lefsky, M.A., Harding, D.J., Keller, M., Cohen, W.B., Carabajal, C.C., Del Bom Espirito-Santo, F., Hunter, M.O., de Oliveira, R., 2005. Estimates of forest canopy height and aboveground biomass using ICESat. Geophys. Res. Lett. 32 (22), 1–4.
Leitold, V., Morton, D. C., Longo, M., dos-Santos, M.N., Keller, M., Scaranello, M., 2018. El Niño drought increased canopy turnover in Amazon forests. New Phytol. 219(3), 959–971.
Leitold, V., Morton, D.C., Martinuzzi, S., Paynter, I., Uriarte, M., Keller, M., Ferraz, A., Cook, B.D., González, G., et al., 2021. Tracking the rates and mechanisms of canopy damage and recovery following Hurricane Maria using multitemporal lidar data. Ecosystems.
Lim, K., Treitz, P., Wulder, M., St-Ongé, B., Flood, M., 2003. LiDAR remote sensing of forest structure. Prog. Phys. Geogr. 27 (1), 88–106.
Lu, J., Wang, H., Qin, S., Cao, L., Pu, R., Li, G., Sun, J., 2020. Estimation of aboveground biomass of Robinia pseudoacacia forest in the Yellow River Delta based on UAV and Backpack LiDAR point clouds. Int. J. Appl. Earth Obs. Geoinf. 86, 102014.
Lugo, A.E., 2008. Visible and invisible effects of hurricanes on forest ecosystems: an international review. Austral Ecol. 33 (4), 368–398.
Lugo, A.E., Snedaker, S.C., 1974. The ecology of mangroves. Annu. Rev. Ecol. Syst. 5 (1), 39–64.
Malmstadt, J., Scheitlin, K., Elsner, J., 2009. Florida hurricanes and damage costs. Southeastern Geographer 49 (2), 108–131.
Maurya, K., Mahajan, S., Chaube, N., 2021. Remote sensing techniques: Mapping and monitoring of mangrove ecosystem—A review. Complex & Intell. Syst. 7 (6), 2797–2818.
Mendelsohn, R., Emanuel, K., Chonabayashi, S., Bakkensen, L., 2012. The impact of climate change on global tropical cyclone damage. Nat. Clim. Change 2 (3), 205–209.
Menéndez, P., Losada, I.J., Torres-Ortega, S., Narayan, S., Beck, M.W., 2020. The global flood protection benefits of mangroves. Sci. Rep. 10 (1), 1–11.
Meyer, V., Saatchi, S.S., Chave, J., Dalling, J.W., Bohlman, S., Fricker, G.A., Robinson, C., Neumann, M., Hubbell, S., 2013. Detecting tropical forest biomass dynamics from repeated airborne lidar measurements. Biogeosciences 10 (8), 5421–5438.
Milbrandt, E.C., Greenawalt-Boswell, J.M., Sokoloff, P.D., Bortone, S.A., 2006. Impact and response of Southwest Florida mangroves to the 2004 hurricane season. Estuaries Coasts 29 (6), 979–984.
Osland, M.J., Feher, L.C., Anderson, G.H., Vervaeke, W.C., Krauss, K.W., Whelan, K.R.T., Balentine, K.M., Tiling-Range, G., Smith, T.J., Cahoon, D.R., 2020. A tropical cyclone-induced ecological regime shift: Mangrove forest conversion to mudflat in Everglades National Park (Florida, USA). Wetlands 40, 1445–1458.
Peereman, J., Hogan, J.A., Lin, T.-C.-C., 2022. Disturbance frequency, intensity and forest structure modulate cyclone-induced changes in mangrove forest canopy cover. Glob. Ecol. Biogeogr. 31 (1), 37–50.
Pham, T.D., Yokoya, N., Bui, D.T., Yoshino, K., Friess, D.A., 2019. Remote sensing approaches for monitoring mangrove species, structure, and biomass: Opportunities and challenges. Remote Sens. 11 (3), 1–24.
Polidoro, B.A., Carpenter, K.E., Collins, L., Duke, N.C., Ellison, A.M., Ellison, J.C., Farnsworth, E.J., Fernando, E.S., Kathiresan, K., Koedam, N.E., et al., 2010. The loss of species: mangrove extinction risk and geographic areas of global concern. PLoS ONE 5 (4), e10095.
Radabaugh, K.R., Moyer, R.P., Chappel, A.R., Powell, C.E., Bociu, I., Clark, B.C., Smoak, J.M., 2018. Coastal blue carbon assessment of mangroves, salt marshes, and salt barrens in Tampa Bay, Florida, USA. Estuaries Coasts 41 (5), 1496–1510.
Radabaugh, K.R., Moyer, R.P., Chappel, A.R., Dontis, E.E., Russo, C.E., Joyse, K.M., Bownik, M.W., Goeckner, A.H., Khan, N.S., 2020. Mangrove Damage, Delayed Mortality, and Early Recovery Following Hurricane Irma at Two Landfall Sites in Southwest Florida, USA. Estuaries Coasts 43 (5), 1104–1118.
Rasquinha, D.N., Mishra, D.R., 2021. Tropical cyclones shape mangrove productivity gradients in the Indian subcontinent. Sci. Rep. 11 (1), 1–12.
Réjou-Méchain, M., Tymen, B., Blanc, L., Fauset, S., Feldpausch, T.R., Monteagudo, A., Phillips, O.L., Richard, H., Chave, J., 2015. Using repeated small-footprint LiDAR acquisitions to infer spatial and temporal variations of a high-biomass Neotropical forest. Remote Sens. Environ. 169, 93–101.
Rifat, S.A., Al, L.W., 2019. Quantifying spatiotemporal patterns and major explanatory factors of urban expansion in Miami Metropolitan Area during 1992–2016. Remote Sens. 11 (21), 2493.
Rivera-Monroy, V.H., Danielson, T.M., Castañeda-Moya, E., Marx, B.D., Travieso, R., Zhao, X., Gaiser, E.E., Farfan, L.M., 2019. Long-term demography and stem productivity of Everglades mangrove forests (Florida, USA): Resistance to hurricane disturbance. For. Ecol. Manage. 440, 79–91.
Ross, M.S., Ruiz, P.L., Sah, J.P., Reed, D.L., Walters, J., Meeder, J.F., 2006. Early post-hurricane stand development in fringe mangrove forests of contrasting productivity. Plant Ecol. 185 (2), 283–297.
Roth, L.C., 1992. Hurricanes and mangrove regeneration: effects of Hurricane Joan, October 1988, on the vegetation of Isla del Venado, Bluefields, Nicaragua. Biotropica 375–384.
Ruiz, P., Perry, C., Garcia, A., Guichardot, M., Foguer, M., Ingram, J., Prats, M., Pulido, C., Shamblin, R., Whelan, K., 2021. The vegetation of Everglades National Park: Final report.
Shiels, A.B., Gonzalez, G., Lodge, D.J., Willig, M.R., Zimmerman, J.K., 2015. Cascading effects of canopy opening and debris deposition from a large-scale hurricane experiment in a tropical rain forest. Bioscience 65 (9), 871–881.
Simard, M., Zhang, K., Rivera-Monroy, V.H., Ross, M.S., Ruiz, P.L., Castañeda-Moya, E., Twilley, R.R., Rodriguez, E., 2006. Mapping height and biomass of mangrove forests in Everglades National Park with SRTM elevation data. Photogramm. Eng. Remote Sens. 72 (3), 299–311.

Simard, M., Fatoyinbo, L., Smetanka, C., Rivera-Monroy, V.H., Castañeda-Moya, E., Thomas, N., Van der Stocken, T., der Stocken, T., 2019. Mangrove canopy height globally related to precipitation, temperature and cyclone frequency. Nat. Geosci. 12 (1), 40–45.

Sippo, J.Z., Lovelock, C.E., Santos, I.R., Sanders, C.J., Maher, D.T., 2018. Mangrove mortality in a changing climate: An overview. Estuar. Coast. Shelf Sci. 215 (May), 241–249.

Smith, T.J., Robblee, M.B., Wanless, H.R., Doyle, T.W., 1994. Mangroves, hurricanes, and lightning strikes. Bioscience 44 (4), 256–262.

Smith, T.J., Anderson, G.H., Balentine, K., Tiling, G., Ward, G.A., Whelan, K.R.T., 2009. Cumulative impacts of hurricanes on Florida mangrove ecosystems: Sediment deposition, storm surges and vegetation. Wetlands 29 (1), 24–34.

Stovall, A.E.L., Fatoyinbo, T., Thomas, N.M., Armston, J., Ebanega, M.O., Simard, M., Trettin, C., Obiang Zogo, R.V., Aken, I.A., Debina, M., Me Kemoe, A.M., Assoumou, E.O., Kim, J.S., Lagomasino, D., Lee, S.-K., Ndong Obame, J.C., Voubou, G.D., Essono, C.Z., 2021. Comprehensive comparison of airborne and spaceborne SAR and LiDAR estimates of forest structure in the tallest mangrove forest on earth. Sci. Remote Sens. 4 (August), 100034.

Svejkovsky, J., Ogurcak, D.E., Ross, M.S., Arkowitz, A., 2020. Satellite image-based time series observations of vegetation response to Hurricane Irma in the lower Florida keys. Estuaries Coasts 43 (5), 1058–1069.

Taillie, P.J., Roman-Cuesta, R., Lagomasino, D., Cifuentes-Jara, M., Fatoyinbo, T., Ott, L. E., Poulter, B., 2020. Widespread mangrove damage resulting from the 2017 Atlantic mega hurricane season. Environ. Res. Lett. 15 (6), 64010.

Thomas, N., Lucas, R., Bunting, P., Hardy, A., Rosenqvist, A., Simard, M., 2017. Distribution and drivers of global mangrove forest change, 1996–2010. PLoS ONE 12 (6), e0179302.

Twilley, R.R., Chen, R., 1998. A water budget and hydrology model of a basin mangrove forest in Rookery Bay, Florida. Mar. Freshwater Res. 49 (4), 309–323.

Twilley, R.R., Chen, R.H., Hargis, T., 1992. Carbon sinks in mangroves and their implications to carbon budget of tropical coastal ecosystems. Water Air Soil Pollut. 64 (1), 265–288.

Twilley, R.R., Rivera-Monroy, V.H., 2005. Developing performance measures of mangrove wetlands using simulation models of hydrology, nutrient biogeochemistry, and community dynamics. J. Coastal Res. 79–93.

Twilley, R.R., Rivera-Monroy, V. rove wetlands. Coastal Wetlands: An Integrated Ecosystem Approach, 641–684.

Vepakomma, U., St-Onge, B., Kneeshaw, D., 2008. Spatially explicit characterization of boreal forest gap dynamics using multi-temporal lidar data. Remote Sens. Environ. 112 (5), 2326–2340.

Walters, B.B., Rönnbäck, P., Kovacs, J.M., Crona, B., Hussain, S.A., Badola, R., Primavera, J.H., Barbier, E., Dahdouh-Guebas, F., 2008. Ethnobiology, socio-economics and management of mangrove forests: A review. Aquat. Bot. 89 (2), 220–236.

Wang, L., Jia, M., Yin, D., Tian, J., 2019. A review of remote sensing for mangrove forests: 1956–2018. Remote Sens. Environ. 231(December 2018).

Wdowinski, S., Bray, R., Kirtman, B.P., Wu, Z., 2016. Increasing flooding hazard in coastal communities due to rising sea level: Case study of Miami Beach, Florida. Ocean Coast. Manag. 126, 1–8.

Wedeux, B., Dalponte, M., Schlund, M., Hagen, S., Cochrane, M., Graham, L., Usup, A., Thomas, A., Coomes, D., 2020. Dynamics of a human-modified tropical peat swamp forest revealed by repeat lidar surveys. Glob. Change Biol. 26 (7), 3947–3964.

Xiong, L., Wang, G., Yan, B., Guo, W., Wang, J., Liu, H., Zhou, X., Sun, X., 2018. Evaluating the accuracy of Airborne Laser Scanning for Mountain Mapping: A Case Study at the Slumgullion Landslide Site in Colorado, US. AGU Fall Meeting Abstracts 2018, G21C–G.

Xiong, L., Wang, G., Bao, Y., Zhou, X., Wang, K., Liu, H., Sun, X., Zhao, R., 2019. A rapid terrestrial laser scanning method for coastal erosion studies: A case study at Freeport, Texas, USA. Sensors 19 (15), 3252.

Yagci, A.L., Santanello, J.A., Jones, J.W., Barr, J., 2017. Estimating evaporative fraction from readily obtainable variables in mangrove forests of the Everglades, USA. Int. J. Remote Sens. 38 (14), 3981–4007.

Zhang, K., 2008. Identification of gaps in mangrove forests with airborne LIDAR. Remote Sens. Environ. 112 (5), 2309–2325.

Zhang, C., Durgan, S.D., Lagomasino, D., 2019a. Modeling risk of mangroves to tropical cyclones: A case study of Hurricane Irma. Estuar. Coast. Shelf Sci. 224 (April), 108–116.

Zhang, K., Chen, S. C., Whitman, D., Shyu, M. L., Yan, J., Zhang, C., 2003. A progressive morphological filter for removing nonground measurements from airborne LIDAR data. IEEE Trans. Geosci. Remote Sens. 41(4 PART I), 872–882.

Zhang, K., Simard, M., Ross, M., Rivera-Monroy, V.H., Houle, P., Ruiz, P., Twilley, R.R., Whelan, K.R.T., 2008. Airborne laser scanning quantification of disturbances from hurricanes and lightning strikes to mangrove forests in everglades national park, USA. Sensors 8 (4), 2262–2292.

Zhang, K., Gann, D., Ross, M., Biswas, H., Li, Y., Rhome, J., 2019b. Comparison of TanDEM-X DEM with LiDAR data for accuracy assessment in a coastal urban area. Remote Sensing 11 (7).

Zhao, X., Rivera-Monroy, V.H., Farfán, L.M., Briceño, H., Castañeda-Moya, E., Travieso, R., Gaiser, E.E., 2021. Tropical cyclones cumulatively control regional carbon fluxes in Everglades mangrove wetlands (Florida, USA). Sci. Rep. 11 (1), 1–17.

Zhao, K., Suarez, J.C., Garcia, M., Hu, T., Wang, C., Londo, A., 2018. Utility of multitemporal lidar for forest and carbon monitoring: Tree growth, biomass dynamics, and carbon flux. Remote Sens. Environ. 204, 883–897.

Zimble, D.A., Evans, D.L., Carlson, G.C., Parker, R.C., Grado, S.C., Gerard, P.D., 2003. Characterizing vertical forest structure using small-footprint airborne LiDAR. Remote Sens. Environ. 87 (2–3), 171–182.